Monthly Notices
of the
ROYAL ASTRONOMICAL SOCIETY

MNRAS **466,** 1372–1381 (2017)
Advance Access publication 2016 December 1

doi:10.1093/mnras/stw3117

The 2004 outburst of BHC H1743-322: analysis of spectral and timing properties using the TCAF solution

Ayan Bhattacharjee,[1]★ Indrani Banerjee,[1] Anuvab Banerjee,[1] Dipak Debnath[2]★ and Sandip K. Chakrabarti[1,2]★

[1]*S. N. Bose National Centre for Basic Sciences, Block-JD, Sector-3, Salt Lake, Kolkata 700106, India*
[2]*Indian Center for Space Physics, 43 Chalantika, Garia St. Road, Kolkata 700084, India*

Accepted 2016 November 29. Received 2016 November 29; in original form 2016 May 21

ABSTRACT

The black hole transient H1743-322 exhibited several outbursts with temporal and spectral variability since its discovery in 1977. These outbursts occur at a quasi-regular recurrence period of around 0.5–2 yr, since its rediscovery in 2003 March. We investigate accretion flow dynamics around the low-mass X-ray binary H1743-322 during its 2004 outburst using the *RXTE* (*Rossi X-Ray Timing Explorer*)/PCA archival data. We use two component advective flow (TCAF) solution to analyse the spectral data. From the fits with TCAF solution, we obtain day-to-day variation of physical accretion rates of Keplerian and sub-Keplerian components, size of the Compton cloud and its other properties. Analysis of the spectral properties of the 2004 outburst by keeping fitted normalization to be in a narrow range and its timing properties in terms of the presence and absence of quasi-periodic oscillations, enable us to constrain the mass of the black hole in a range of 10.31 $M_\odot$–14.07 $M_\odot$ that is consistent with other estimates reported in the literature.

Key words: accretion, accretion discs – radiation: dynamics – shock waves – stars: black holes – stars individual: (H 1743-322) – X-rays: binaries.

1 INTRODUCTION

The advent of X-ray astronomy and the launch of *Rossi X-Ray Timing Explorer* (*RXTE*) since the last two decades have significantly enhanced our understanding about the accretion processes around compact sources, such as black holes (BHs) and neutron stars (NSs). Most of these compact sources are in binaries, with the NS or the BH as the primary that accretes matter from the companion star (secondary) either by Roche lobe overflow or by capturing the mass lost from the secondary in the form of winds. Due to the presence of turbulent viscosity, a part of the gravitational potential energy lost by the accreting matter is emitted in the form of radiations, chiefly in the soft X-ray domain. Even when significant viscosity is absent, stored thermal energy is lost in X-ray domain by inverse Comptonization. An outbursting black hole candidate (BHC) primarily exhibits four different spectral states, namely, hard state (HS), hard-intermediate state (HIMS), soft-intermediate state (SIMS) and soft state (SS; e.g. McClintock & Remillard 2006; Nandi et al. 2012; Debnath, Chakrabarti & Nandi 2013). Simultaneous analysis of the timing properties of these BHCs reveal that low-frequency quasi-periodic oscillations (QPOs) are also evident in the power density spectra (PDS) of these objects (e.g. Remillard & McClintock 2006). Evolution of spectral and temporal characteristics of several BHCs during their outbursts have been extensively studied (e.g. McClintock & Remillard 2006; Nandi et al. 2012). It has been noted that the various spectral states can be related to different branches of the hardness intensity diagram (HID; Belloni et al. 2005 and Debnath et al. 2008) or, in a more physical hysteresis diagram using accretion rate ratio and X-ray intensity (ARRID; Mondal, Debnath & Chakrabarti 2014; Jana et al. 2016). The HID or the ARRID shows the objects in different spectral states, generally, in the sequence: HS → HIMS → SIMS → SS → SIMS → HIMS → HS. It is well established that in order to interpret majority of BH spectra two types of spectral components, namely, a multicolour blackbody component and a power-law component are needed. The multicolour blackbody component seems to originate from an optically thick, geometrically thin Keplerian flow (Shakura & Sunyaev 1973, hereafter SS73) while the power-law tail of the spectrum is believed to be emanated from a 'Compton' cloud (Sunyaev & Titarchuk 1980, 1985). Several theoretical and phenomenological models ranging from a magnetic corona (Galeev, Rosner & Vaiana 1979) to a hot gas corona over the disc (Haardt & Maraschi 1993; Zdziarski et al. 2003) to a two component advective flow (TCAF) solution (Chakrabarti & Titarchuk 1995, hereafter CT95) exist in the literature that attempts to explain the spectrum and expound the nature and origin of this 'Compton' cloud. In this paper, we use the TCAF solution to investigate the spectral and timing properties of the source during its 2004 outburst.

★ E-mail: ayan12@bose.res.in (AB); dipak@csp.res.in (DD); chakraba@bose.res.in (SKC)

The Galactic transient low-mass BHXB H1743-322 is located at R.A. = $17^{h}46^{m}15^{s}.61$ and Dec = $-32^{\circ}14'00''.6$ (Gursky et al. 1978). The discovery of this source goes back to1977 August–September, when Kaluzienski & Holt (1977) reported its first X-ray activity with the *Ariel V* All Sky Monitor. This was subsequently followed by observations from the *HEAO I* satellite (Doxsey et al. 1977). Further activities of the source in the X-ray band 12–180 keV were observed during the 1977-78 outbursts with the *HEAO I* satellite (Cooke et al. 1984). Based on the colour–colour diagram, obtained from the spectral data of the *HEAO I* satellite, White & Marshall (1984) classified the source to be a potential BHC. Since its first detection, it remained in the quiescent state till 1984 when *EXOSAT* observations reported X-ray activities (Reynolds 1999) that was subsequently followed by detection of activities by TTM/COMIS instruments on board MirKvant in 1996 (Emelyanov, Aleksandrovich & Sunyaev 2000). On 2003 March 21, the *INTEGRAL* satellite detected a bright source named IGR J17464-3213 (Revnivtsev et al. 2003) that displayed X-ray activities and later, *RXTE* confirmed the presence of such an activity from the same region in the sky (Markwardt & Swank 2003) validating the source to be H1743-322. Since 2003, it exhibited several X-ray activities with quasi-regular intervals of about one to two years. In order to investigate multiwavelength properties of the source, it was comprehensively monitored in X-rays (Parmar et al. 2003; Remillard & McClintock 2006; McClintock et al. 2009), IR (Steeghs et al. 2003) and in radio bands (Rupen, Mioduszewski & Dhawan 2003) during its 2003 outburst. McClintock et al. (2009) and Miller-Jones et al. (2012) eventually followed up further investigations of the source in the multiwavelength during its 2003 and 2009 outbursts, respectively.

The mass of the BHC in H1743-322 has not yet been dynamically measured, although several attempts have been made to predict the mass of the BH. Analysing the 2003 outburst data, Shaposhnikov & Titarchuk (2009, hereafter ST09) calculated mass of this BHC to be 13.3 ± 3.2 $M_{\odot}$ using their QPO frequency–photon index correlation method. McClintock et al. (2009) estimated its mass to be $\sim$11 $M_{\odot}$ using their high-frequency QPO correlation method. From the model of high-frequency QPOs based on the mass-angular momentum (i.e. spin of the BH), Pétri (2008) predicted that its mass should lie in the range of 9–13 $M_{\odot}$. Based on its spectral and timing properties using two recent outbursts Molla et al. (2017, hereafter M17) estimated the mass of the BHC to be $M_{\rm BH} = 11.21^{+1.65}_{-1.96}$. These authors also used the method of ST09 and narrowed down the range to $11.65 \pm 0.67\,M_{\odot}$. The source is reported to be at a distance of 8.5 ± 0.8 kpc with the inclination angle of $\theta \sim 75^{\circ} \pm 3^{\circ}$. Steiner, McClintock & Reid (2012) also constrains to the spin a of the source, $-0.3 < a < 0.7$ with a 90 per cent confidence level.

Recent outbursts of H1743-322 in 2010 and 2011 again showed the characteristic state transitions (Shaposhnikov 2010; Shaposhnikov & Tomsick 2010; Debnath et al. 2013) as observed in other outburst sources (Nandi et al. 2012). It was pointed out by Debnath, Chakrabarti & Nandi (2010) that depending upon the outburst light-curve profiles, there are mainly two types of outbursting BHCs: the 'fast-rise slow-decay' (FRSD) type and the 'slow-rise slow-decay' (SRSD) type. The source H1743-322 belongs to the first category. Debnath et al. (2013) investigated the average temporal and spectral properties of the object using combined disc blackbody (DBB) and power law (PL) model using data of 2010 and 2011 outbursts. Mondal et al. (2014) analysed the *RXTE*/PCA data during its 2010 outburst using the TCAF solution allowing the normalization N of the TCAF model to vary in order to get the best fit. On the other hand, M17 analysed the data of H1743-322 using the TCAF solution during its 2010 and 2011 outbursts, restricting the normalization N within a narrow range to estimate the mass of the central object. Here, we follow the same procedure of M17 and M16 to analyse the 2004 outburst of H1743-322 that not only enables us to understand the underlying accretion flow dynamics but also allows us to give a fresh estimate to the mass of the BHC H1743-322. We first determine the average value of normalization by keeping it free within a narrow range. The constant, averaged value of the normalization is then used to refit the spectral data and estimate the mass of the BHC. The 2008b outburst was a 'failed outburst' and hence was not analysed. The 2005 outburst could not be analysed due to lack of data (Coriat et al. 2011). The outburst in 2003 had significant radio activity, which is currently being analysed by Chakrabarti et al. (in preparation). From the rest of the cases, the 2004 outburst was the most prominent one, in terms of total flux and duration. Hence, we selected this 117 d long 2004 outburst for our analysis.

Since several outbursts have already been studied, one could surmise that analysis of yet another outburst would be of limited use. If one observed the sequence of outbursts, the one in 2003 took place after about 20 yr and after that there are quasi-regular outbursts, some very small and some moderate. The one in 2003 is very anomalous in the sense that its intensity was more than five times larger than the next prominent ones, such as those in 2004, 2010 and 2011 and at least 10–15 times stronger than several others. This is probably an indication that the 2003 outburst could have been triggered by a non-linear instability and the system is slowly settling and relaxing after subsequent outbursts, probably before going to a long quiescence state again. It is thus no surprise that ST09 estimation of mass of the 2003 outburst had a huge error margin while M17 estimate using the same method but 2010 and 2011 data shows a narrower margin. Assuming the 2003 outburst is truly anomalous, the first stereotypical outburst is in 2004 and it is important to study this. While fitting the spectra, we find that it is highly soft in much of the time where a standard disk is enough to fit the data. The region where both spectral components are seen prominently, and both the flow components are important is in the declining state. So, we concentrate only on the declining state of the 2004 data.

Judging from the fact that in initial outbursts, the source was going to very bright SSs and then more relative times have been spent in harder states, every outburst can be thought to be separately important and the combination of the evolution of physical parameters may lead to the understanding of the long term behaviour of the system. Furthermore, from the light curves it is easy to see that decay time-scales and peak fluxes are different and both of these parameters are governed by viscosity in the Keplerian flow. The pattern of mass accretion rate variations are also found to be different from one outburst to the other. Even the accuracy of the estimated mass is vastly different for the same method (M17). Thus it is essential that every outburst be studied as accurately as possible.

We organize the paper in the following way. In Section 2, we discuss the salient features of the TCAF solution and the propagatory oscillatory shock (POS) model. In Section 3, we discuss observation and methods of data analysis implementing HEASARC's HEASOFT software package. In Section 4, we present the results obtained from the spectral analysis using the TCAF solution and the POS model. Finally, in Section 5, we conclude with a brief discussion summarizing our main findings with some remarks for future work.

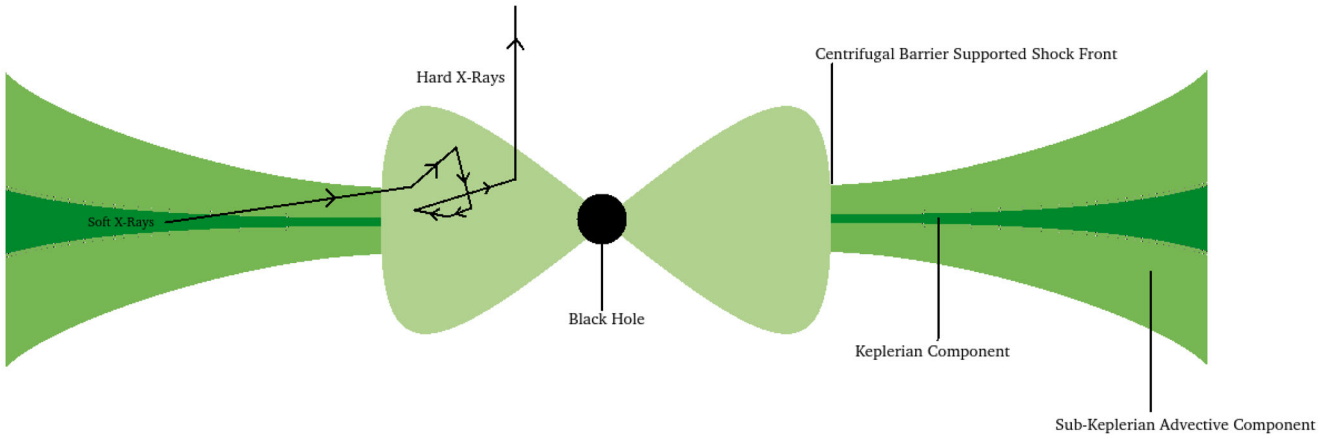

Figure 1. A schematic diagram of the accretion flow dynamics and radiation processes in a TCAF solution. Adapted from CT95.

2 METHOD OF ANALYSIS

2.1 The TCAF solution

Prior to the launch of *RXTE*, CT95 explored the well-established solution of a transonic flow (see Chakrabarti 1990, 1996, hereafter C90, C96) and proposed that the accretion flow generally exhibits a two-component behaviour, namely, a viscous Keplerian flow sandwiched by a weakly viscous sub-Keplerian flow (Fig. 1). This solution, popularly known as the TCAF solution in the literature enunciates that the sub-Keplerian halo component, envelops the Keplerian disc and since it requires negligible viscosity to accrete, falls into the BH with a much higher radial velocity (Soria et al. 2001; Smith, Heindl & Swank 2002; Wu et al. 2002; Cambier & Smith 2013; Tomsick et al. 2014). The sub-Keplerian flow is advective, can reach supersonic speeds and has angular momentum less than that of a Keplerian distribution. Hence, it undergoes a centrifugal pressure supported shock transition to become subsonic in between the two sonic points. The complete solutions are worked out in detail in Chakrabarti 1989 (hereafter C89), and C96. The centrifugal pressure impedes the flow and as a result a standing or oscillating shock is formed depending on whether the Rankine–Hugoniot conditions are satisfied (C89, C96). Thus, the flow puffs up in the vertical direction, and forms the CENtrifugal pressure dominated BOundary Layer (CENBOL). This CENBOL acts as the Comptonizing cloud that upscatters the seed blackbody photons coming from the Keplerian disc. In the natural HS of a BHC, this is the only component that is present. The component near the equatorial plane has a viscosity higher than the critical value and is Keplerian in nature having the characteristics of a standard disc. This component is not always present close to the BH. When the outburst is triggered by increase of matter and viscosity, this disc formation is initiated from outside and it moves in on a daily basis, increasing the supply of Keplerian matter as well as soft seed photons that are intercepted by the CENBOL and are inverse-Comptonized through repeated scattering. A typical route of the photon emerging from the Keplerian disc to the observer via CENBOL is shown in Fig. 1. Initially, the HS is formed when the rates were still low and shock front was hundreds of Schwarzschild radii away and the advective (halo) component rate increases first due to its short infall time. Subsequently, the Keplerian rate starts to increase since its angular momentum is high and it is to be transported by viscosity. Here, the object goes to HIMSs. The rate continues to rise and the cooling time-scale inside CENBOL starts to be smaller compared to the infall time-scale when the condition of oscillation of the shock front is violated and the QPO seen thus far, becomes sporadic and state becomes SIMS. Finally, if Keplerian matter supply is really high, and the viscosity can transport angular momentum very efficiently, soft photons overwhelmingly cools the CENBOL removing it altogether and the SS is produced. This gradual transformation of the size and shape of the CENBOL is clearly depicted in Fig. 2. When the companion turns off the active phase, the process is reversed albeit in a different time-scale. Thus, by giving a clear theoretical origin of the Compton cloud (CENBOL) and self-consistently amalgamating the synergy and the inter-conversion of the two components through viscosity, the TCAF solution provides a clear picture of the entire outburst process and obviates the need of phenomenological models in the subject.

For the calculations, all the equations are reduced to their dimensionless forms. The important references can be found in C89 (hydrodynamical equations), CT95 (spectral, radiative transfer equations), Debnath, Mondal & Chakrabarti (2015a). The last one is the first paper after inclusion of TCAF in XSPEC, where important equations (equations 1–5) of the TCAF solutions are summarized.

Lengths are measured in units of $r_S = 2GM_{\rm BH}/c^2$ (G and c being gravitational constant and the velocity of light), and the accretion rates are measured in units of Eddington rate (also a function of the BH mass $M_{\rm BH}$). The disc accretion rate ($\dot{m}_d$), the halo accretion rate ($\dot{m}_h$), the shock location (X_s), the shock compression ratio (R) and the mass of the BHC ($M_{\rm BH}$) are taken as input parameters and a resulting spectrum is generated. The first four parameters are dependent on the flow properties. Hence, their time-variation reveals the accretion flow dynamics around the object during an outburst. Numerical simulations (Giri & Chakrabarti 2013) and spectral studies (Ghosh et al. 2011) of BHCs reveal that the TCAF solution is the most general solution for accreting matter on to a BH. Self-consistency and stability check of the transonic solution by Giri & Chakrabarti (2013) and Mondal & Chakrabarti (2013)

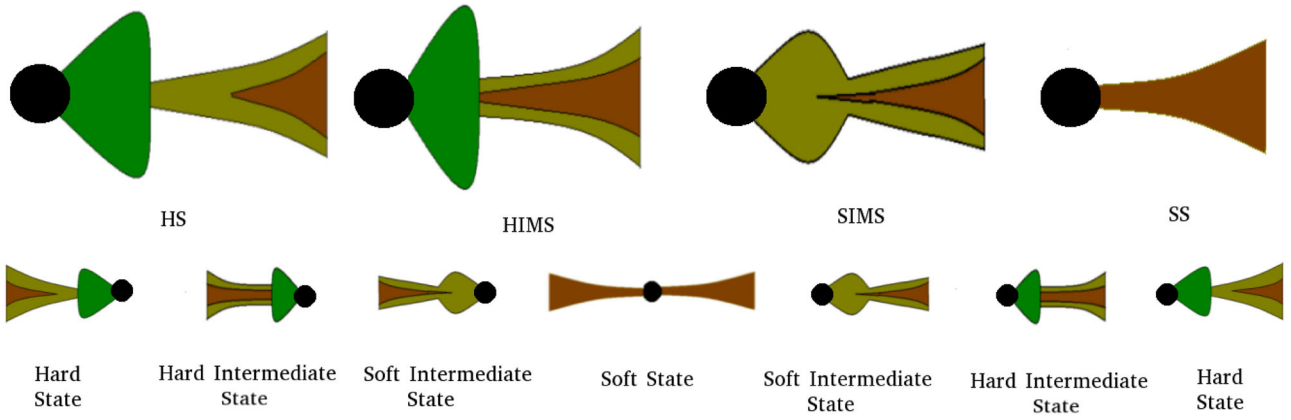

Figure 2. A schematic diagram showing the evolution of the CENBOL and the Keplerian disc in a TCAF solution. At the onset of an outburst, the halo is dominant and the shock front is far away (hard state: HS). The Keplerian component moves inward, cooling the CENBOL and making it smaller (hard intermediate: HIMS). For high disc accretion rate, first the CENBOL cools and QPOs became sporadic (soft intermediate state: SIMS) and finally the halo component is cooled down totally (soft state: SS). The reverse sequence follows when the supply at the outer edge halted. Adapted from Chakrabarti (2016).

corroborate that an advective flow will eventually give rise to a TCAF solution (CT95) when viscous stress near the equatorial plane is substantial. This solution therefore invokes two types of energy extraction processes into a single coherent framework: (i) viscous dissipation in the Keplerian component to produce soft X-rays and (ii) inverse Comptonization of these soft photons to produce hard photons by stored thermal energy in the weakly viscous CENBOL.

After obtaining the shape of the overall spectra, suitable model normalization N is used to raise or lower it to match the observed spectra. In diskbb plus powerlaw model, the normalization comes only from the disc integrated photon number that is used to obtain the inner edge of the truncated disc. In the TCAF fits, one cannot separate the blackbody and power-law components since the disc radiation and its Comptonized spectrum are summed up along with the reflected components in the fits file. The information about the inner edge of the truncated disc is in determining the shock location that is also the outer edge of the Compton cloud (CENBOL). Since this information is already fed into the grid of the fits file, we only require a constant normalization that is primarily mass ($M_{\rm BH}$), distance (D in units of 10 kpc) and inclination angle (i) dependent through a functional relation $N \sim [r_S^2/4\pi D^2]\sin(i)$ (Molla et al. 2016, hereafter M16). Error in mass determination would give rise to error in normalization. Ideally if the CENBOL was lying in a plane, the inclination angle would be globally constant, unless the disc is precessing (which we do not assume here). Also, $M_{\rm BH}$ should not vary over the time-scales of observation. Since $M_{\rm BH} \sim T^4$, and the spectral fits are sensitive to the temperature T, a small error in determination of T gives rise to a significant error in $M_{\rm BH}$. This in turn is reflected in the normalization. Moreover, there can be changes in the peak flux with spectral states when the CENBOL changes its shape and size self-consistently. The variation of flux is due to the variation of accretion rates ($\dot{m}_d$ *and* $\dot{m}_h$), shock location (X_s) and compression ratio (R). In any case, our result is independent of the exact value of normalization, and our requirement is that it may remain in a narrow range so that we are certain the fitting routine stays in the same global minimum. The average value, for statistical reasons, is taken as the constant value of normalization for the outburst and the entire study is repeated with this constant normalization. Under this assumption, if the $M_{\rm BH}$ fluctuates, D and i have to adjust to ensure a constant N, though that does not affect our analysis. For all practical purposes, this N is 'fixed' from one outburst to the other as it should be when precession of the disc is absent.

Recently, the TCAF model (CT95; Chakrabarti 1997) has been successfully incorporated in HEASARC's spectral analysis software package XSPEC (Arnaud 1996) as a local additive table model (Debnath, Chakrabarti & Mondal 2014; Mondal, Debnath & Chakrabarti 2014; Debnath et al. 2015a,b; Chatterjee et al. 2016; Jana et al. 2016; Mondal, Chakrabarti & Debnath 2016; M16). It accomplishes fitting of the spectral data of several transient BHCs (e.g. H 1743-322, GX 339-4, MAXI J1659-152, MAXI J1836-194), during their X-ray outbursts which in turn enables us to get a much clearer picture of the accretion flow dynamics in terms of the disc and halo mass accretion rates, the location and size of the Comptonizing cloud (here, CENBOL) and the strength of the shock, which in conjunction with the size and halo rate gives an idea of the optical depth.

2.2 POS model

Once the Keplerian disc is formed, the CENBOL is cooled down gradually. If the cooling time-scale of the CENBOL lies within ~50 per cent of the infall time-scale from the shock front to the BH, a resonance occurs when the shock or the outer edge of the Compton cloud starts to oscillate (Molteni, Sponholz & Chakrabarti 1996; Chakrabarti & Manickam 2000; Chakrabarti, Mondal & Debnath 2015). The oscillation of the shock front leads to the generation of low-frequency quasi-periodic oscillations (QPOs) in the PDS of the light curves. Due to variation of shock conditions with the changes in disc and halo accretion rates, the average shock location moves inwards (outwards) for the rising (declining) phase of the outburst (Fig. 2). Simultaneously, the QPO frequencies evolve as well.

The frequency of oscillation of the shock front, which in turn is related to the QPO frequency ($\nu_{\rm qpo}$) is obtained from the inverse of the infall time ($t_{\rm infall}$). If, c is the speed of light, G is the gravitational constant and $M_{\rm BH}$ is the mass of the BH, then the unit of frequency is given by, $\nu_{s0} = \frac{c^3}{2GM_{\rm BH}}$. The QPO frequency is then written as,

$$\nu_{\rm qpo} = \nu_{s0}/t_{\rm infall} = \frac{c^3}{2GM_{\rm BH}} \frac{1}{[RX_s(X_s-1)^{1/2}]}$$

where, R is the shock compression ratio and X_s is the shock location in units of r_S (Chakrabarti et al. 2008; Chakrabarti, Dutta & Pal 2009; Debnath et al. 2010, 2013; Nandi et al. 2012).

According to the POS model, the shock location varies with time as

$$X_s(t) = X_s(0) \pm t v_0 / r_S,$$

where v_0 and $X_s(0)$ are the initial location and velocity of the shock. The plus (minus) sign is associated with the shock front for declining (rising) phase. This can, in turn, be used to determine the mean radial velocity of the shock front during the outburst that further enables us to study the evolution of X_s and hence the evolution of the QPO frequencies. The POS model has a parametric dependence on the mass $M_{\rm BH}$. Hence, if QPOs are observed in a series of consecutive days, then the POS model can be used to fit the variation of the QPO frequency with time. The value of mass that gives the best fit to the data will be the mass of the BH.

3 OBSERVATION AND DATA ANALYSIS

RXTE/PCA covered the 2004 outburst of H1743-322 spanning from 2004 July 11 (MJD = 53197.287) to 2004 November 5 (MJD = 53314.749). 42 observations were recorded by *RXTE* during the aforementioned period with an average gap of ∼3 d between consecutive observations. We use HEASARC's software package HEASOFT, version HEADAS 6.18 and XSPEC version 12.9.0 to carry out our data analysis procedure. In order to generate the source and the background '.pha' files and fit the spectrum exploiting the TCAF solution we follow the procedure adopted by Debnath et al. (2013, 2014). For spectral analysis, the Standard2 mode Science Data of PCA (FS4a*.gz) were used. Spectra from all the Xenon layers of PCU2 consisting of 128 channels (without any binning/grouping of the channels) were extracted for all the observational IDs. Dead-time and PCA breakdown correction were incorporated in our analysis. We extracted the PCA background by applying the command 'runpcabackest' and by using the latest bright-source background model. In order to take care of the South Atlantic Anomaly (SAA) data, we incorporated the PCA SAA history file. The task 'pcarsp' was used to create the response files. For preparing the PDS, all active PCUs were used for a broad energy binned between 0 and 35 channel data. The 2.5–25 keV PCA spectra of these observation IDs with appropriate background subtraction were fitted with the TCAF solution based additive model fits file. To accomplish the best fit, a Gaussian line was used to model the iron line emission. Throughout the outburst, the hydrogen column density (N_H) was kept fixed at 1.6×10^{22} atoms cm^{-2} (Capitanio et al. 2009) for absorption model *wabs*. A systematic instrumental error of 1 per cent was assumed. We used 'err' command to find out 90 per cent confidence error values in model fitted parameters.

Here, we initially fit the entire 117 d long outburst using wabs*(diskbb+PL) model. Next, we fit the last 27 d of the outburst (declining phase) by keeping $\dot{m}_d$, $\dot{m}_h$, X_s and $M_{\rm BH}$ free and normalization within the range $10 < N < 20$ as in M17. Next, using the POS model, the velocity of the shock front was found out using the parameters as obtained from the previous analysis. The same process of spectral fits using the TCAF model was repeated using the average value of normalization obtained from the previous analysis. For this purpose, the model fits file (TCAF.fits) was used that uses the theoretical spectra-generating software by varying the five basic input parameters in the suitably upgraded CT95 code and is then incorporated in the XSPEC as a local additive model. The version of TCAF used for fitting the spectra in this work is TCAFv0.1.R3.fits used in Debnath et al. (2015a) and references therein.

4 RESULTS

In this section, we present the results obtained from the analysis of the data of H1743-322 during the 2004 outburst by the TCAF fits.

A comparison of *RXTE*/ASM light curves of H1743-322 between 2003 and 2009 shows that the source predominantly resided in the softer states during the 2004 outburst, namely, SS and SIMS and only towards the end of the outburst the source entered in the HIMS and HS (Fig. 3e). Capitanio et al. (2005) also reports a similar behaviour of the source during this outburst.

Figs 3(a) and (b), illustrate variation of *diskbb* temperature $T_{\rm in}$ and the *powerlaw* photon index Γ with MJD. Figs 3(c) and (d) show the variation of the flux contributed by *diskbb* and *powerlaw* models, respectively, while Fig. 3(e) shows the variation of the total spectral flux. The ratio of *diskbb* flux ($\rm Flux_{diskbb}$) and *powerlaw* flux ($\rm Flux_{PL}$), ($\rm Ratio_{flux}$) is shown in the panel 3(f). The variation of the inner edge of the disc ($\rm R_{in}$), given by the diskbb normalization with MJD is shown in Fig. 3(g). We calculated the individual flux contributions for the *diskbb* and the *powerlaw* components by using the convolution model 'cflux' once for the *diskbb* and then for the *powerlaw*, to fit the spectra in the 2.5–25 keV energy band. The analysis with *wabs*(diskbb+powerlaw)* model also reveals that the data for the rising phase was only obtained well after the object settled into SIMS. Subsequently, during the rising phase, the peak and the initial part of the declining phase of the outburst the underlying

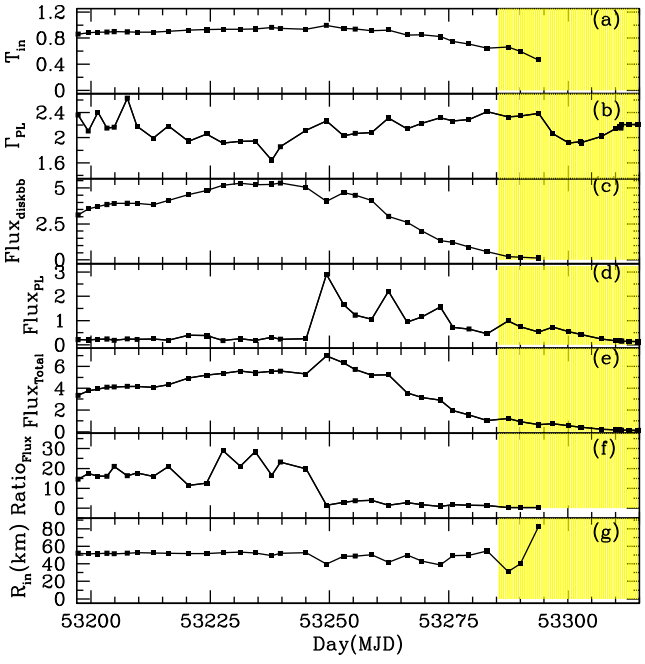

Figure 3. Variation of (a) the *diskbb* Temperature ($T_{\rm in}$) in units of keV, (b) the *power law* photon index (Γ), (c) the *diskbb* flux ($\rm Flux_{diskbb}$) in units of 10^{-9} ergs cm^{-2} s^{-1}, (d) the *powerlaw* flux ($\rm Flux_{PL}$) in units of 10^{-9} ergs cm^{-2} s^{-1}, (e) the total flux ($\rm Flux_{Total}$) in units of 10^{-9} ergs cm^{-2} s^{-1}, (f) the ratio of *diskbb* flux ($\rm Flux_{diskbb}$) and *powerlaw* flux ($\rm Flux_{PL}$), $\rm Ratio_{flux}$ and (g) the inner edge of the disc ($R_{\rm in}$) in units of km, given by the diskbb normalization with MJD (d). All the above variations are in the 2.5–25 keV energy band. The declining phase, which was fitted with the TCAF solution, is shaded with yellow. [A colour version of this figure is available in the online version.]

Table 1. TCAF model fitted parameters in 2.5–25 keV energy band for normalization in the range 10–20. Here, we list the variations of disc accretion rate ($\dot{m}_d$) and halo accretion rate ($\dot{m}_h$) in Eddington units, shock location (X_s) in Schwarzschild radius, shock compression ratio (R), mass of the BHC ($M_{\rm BH}$) in $M_\odot$ and model normalization (N) with MJD along with their errors. The reduced χ^2 values for each case is also shown in the last column.

Obs.	Id.	MJD	$\dot{m}_{\rm d}$ ($\dot{M}_{\rm Edd}$)	$\dot{m}_h$ ($\dot{M}_{\rm Edd}$)	X_s (r_S)	R	$M_{\rm BH}$ ($M_\odot$)	N	χ^2/dof
1	X − 02 − 00	53287.484	$0.785^{+0.108}_{-0.028}$	$0.070^{+0.017}_{-0.001}$	$29.790^{+0.019}_{-0.019}$	$1.070^{0+0.001}_{-0.001}$	$13.774^{+0.143}_{-0.141}$	$19.496^{+0.165}_{-0.164}$	37.41/40
2	X − 02 − 01	53290.036	$0.649^{+0.007}_{-0.007}$	$0.064^{+0.001}_{-0.001}$	$28.862^{+0.023}_{-0.023}$	$1.063^{+0.002}_{-0.001}$	$14.611^{+0.127}_{-1.253}$	$17.481^{+0.304}_{-0.303}$	44.00/40
3	X − 03 − 00	53293.882	$0.617^{+0.055}_{-0.021}$	$0.059^{+0.005}_{-0.008}$	$27.803^{+0.032}_{-0.032}$	$1.055^{+0.001}_{-0.001}$	$14.700^{+0.176}_{-0.438}$	$13.242^{+0.120}_{-0.120}$	39.04/40
4	X − 03 − 10	53296.834	$0.041^{+0.004}_{-0.004}$	$0.128^{+0.004}_{-0.009}$	$75.662^{+0.704}_{-0.699}$	$2.804^{+0.010}_{-0.010}$	$13.995^{+0.151}_{-0.149}$	$10.856^{+0.102}_{-0.102}$	40.92/40
5	X − 04 − 00	53300.208	$0.027^{+0.001}_{-0.0003}$	$0.139^{+0.001}_{-0.002}$	$84.784^{+1.265}_{-1.249}$	$3.717^{+0.046}_{-0.046}$	$10.476^{+0.091}_{-0.090}$	$13.355^{+0.156}_{-0.155}$	41.69/40
6	X − 04 − 10	53302.689	$0.026^{+0.0003}_{-0.005}$	$0.140^{+0.055}_{-0.001}$	$93.115^{+1.528}_{-1.506}$	$3.660^{+0.158}_{-0.134}$	$10.112^{+0.106}_{-0.105}$	$11.228^{+0.171}_{-0.171}$	35.92/40
7	X − 04 − 20	53302.829	$0.025^{+0.007}_{-0.003}$	$0.140^{+0.004}_{-0.003}$	$95.118^{+0.657}_{-0.654}$	$3.745^{+0.022}_{-0.021}$	$9.981^{+0.044}_{-0.044}$	$10.480^{+0.072}_{-0.071}$	31.09/40
8	X − 05 − 00	53307.032	$0.021^{+0.005}_{-0.003}$	$0.120^{+0.001}_{-0.001}$	$114.867^{+0.737}_{-0.733}$	$3.519^{+0.024}_{-0.028}$	$10.517^{+0.150}_{-0.140}$	$11.121^{+0.250}_{-0.249}$	31.58/40
9	X − 05 − 01	53309.956	$0.022^{+0.004}_{-0.004}$	$0.111^{+0.017}_{-0.010}$	$133.474^{+1.572}_{-1.556}$	$3.505^{+0.032}_{-0.032}$	$10.094^{+0.204}_{-0.200}$	$13.625^{+0.238}_{-0.238}$	17.51/40
10	X − 05 − 03	53310.876	$0.021^{+0.004}_{-0.003}$	$0.115^{+0.015}_{-0.010}$	$145.277^{+1.281}_{-1.273}$	$3.309^{+0.023}_{-0.023}$	$12.873^{+0.229}_{-0.224}$	$12.815^{+0.204}_{-0.203}$	32.10/40
11	X − 05 − 10	53311.146	$0.021^{+0.004}_{-0.001}$	$0.127^{+0.006}_{-0.016}$	$149.990^{+1.338}_{-1.329}$	$3.267^{+0.021}_{-0.021}$	$12.167^{+0.192}_{-0.189}$	$12.638^{+0.194}_{-0.194}$	23.74/40
12	X − 05 − 02	53311.306	$0.021^{+0.014}_{-0.004}$	$0.126^{+0.002}_{-0.003}$	$162.910^{+3.033}_{-2.980}$	$3.041^{+0.053}_{-0.052}$	$14.133^{+0.613}_{-0.641}$	$14.016^{+0.550}_{-0.549}$	33.27/40
13	X − 05 − 04	53312.736	$0.020^{+0.008}_{-0.002}$	$0.128^{+0.010}_{-0.024}$	$168.780^{+2.106}_{-2.078}$	$3.237^{+0.033}_{-0.033}$	$12.504^{+0.365}_{-0.354}$	$15.540^{+0.423}_{-0.422}$	31.36/40
14	X − 06 − 00	53314.749	$0.020^{+0.007}_{-0.002}$	$0.127^{+0.007}_{-0.022}$	$171.966^{+2.146}_{-1.900}$	$3.135^{+0.025}_{-0.032}$	$13.108^{+0.334}_{-0.325}$	$15.217^{+0.345}_{-0.344}$	18.94/40

Table 2. TCAF model fitted parameters in 2.5–25 keV energy band for normalization, $N = N_{\rm avg} = 13.65$. Here, we list the variations of disc accretion rate ($\dot{m}_d$) and halo accretion rate ($\dot{m}_h$) in Eddington units, shock location (X_s) in units of Schwarzschild radius, shock compression ratio (R) and mass of the BHC ($M_{\rm BH}$) in $M_\odot$ with MJD, along with their errors. The reduced χ^2 values for each case is also shown in the last column.

Obs.	Id.	MJD	$\dot{m}_{\rm d}$ ($\dot{M}_{\rm Edd}$)	$\dot{m}_h$ ($\dot{M}_{\rm Edd}$)	X_s (r_S)	R	$M_{\rm BH}$ ($M_\odot$)	N	χ^2/dof
1	X − 02 − 00	53287.484	$0.771^{+0.065}_{-0.022}$	$0.068^{+0.008}_{-0.0003}$	$29.153^{+0.027}_{-0.027}$	$1.079^{0+0.001}_{-0.001}$	$14.852^{+0.130}_{-0.128}$	13.65	36.81/41
2	X − 02 − 01	53290.036	$0.730^{+0.020}_{-0.019}$	$0.061^{+0.001}_{-0.002}$	$28.808^{+0.025}_{-0.025}$	$1.075^{+0.001}_{-0.001}$	$14.491^{+0.165}_{-0.216}$	13.65	44.12/41
3	X − 03 − 00	53293.882	$0.615^{+0.050}_{-0.012}$	$0.059^{+0.003}_{-0.009}$	$27.768^{+0.032}_{-0.032}$	$1.054^{+0.001}_{-0.001}$	$14.594^{+0.167}_{-0.125}$	13.65	38.71/41
4	X − 03 − 10	53296.834	$0.039^{+0.004}_{-0.004}$	$0.110^{+0.006}_{-0.004}$	$79.041^{+0.494}_{-0.491}$	$3.026^{+0.016}_{-0.016}$	$12.772^{+0.127}_{-0.126}$	13.65	40.40/41
5	X − 04 − 00	53300.208	$0.027^{+0.003}_{-0.003}$	$0.139^{+0.016}_{-0.018}$	$81.732^{+1.278}_{-1.260}$	$3.700^{+0.046}_{-0.046}$	$10.095^{+0.082}_{-0.081}$	13.65	41.68/41
6	X − 04 − 10	53302.689	$0.024^{+0.002}_{-0.008}$	$0.119^{+0.017}_{-0.015}$	$93.727^{+1.872}_{-1.838}$	$3.963^{+0.034}_{-0.033}$	$9.356^{+0.061}_{-0.061}$	13.65	35.63/41
7	X − 04 − 20	53302.829	$0.026^{+0.004}_{-0.001}$	$0.130^{+0.009}_{-0.007}$	$94.085^{+1.076}_{-1.068}$	$3.883^{+0.086}_{-0.084}$	$9.831^{+0.034}_{-0.034}$	13.65	30.09/41
8	X − 05 − 00	53307.032	$0.017^{+0.004}_{-0.001}$	$0.128^{+0.018}_{-0.020}$	$113.569^{+0.793}_{-0.788}$	$3.538^{+0.014}_{-0.028}$	$10.268^{+0.153}_{-0.151}$	13.65	31.19/41
9	X − 05 − 01	53309.956	$0.022^{+0.004}_{-0.004}$	$0.111^{+0.017}_{-0.010}$	$133.302^{+1.573}_{-1.557}$	$3.510^{+0.032}_{-0.032}$	$10.082^{+0.204}_{-0.199}$	13.65	17.51/41
10	X − 05 − 03	53310.876	$0.021^{+0.004}_{-0.003}$	$0.114^{+0.013}_{-0.010}$	$145.746^{+1.276}_{-1.270}$	$3.321^{+0.023}_{-0.023}$	$12.488^{+0.208}_{-0.205}$	13.65	32.10/41
11	X − 05 − 10	53311.146	$0.020^{+0.004}_{-0.001}$	$0.127^{+0.006}_{-0.016}$	$150.742^{+1.335}_{-1.326}$	$3.281^{+0.021}_{-0.021}$	$11.700^{+0.177}_{-0.174}$	13.65	23.75/41
12	X − 05 − 02	53311.306	$0.022^{+0.001}_{-0.001}$	$0.125^{+0.002}_{-0.003}$	$154.643^{+3.178}_{-3.117}$	$2.957^{+0.050}_{-0.050}$	$12.867^{+0.562}_{-0.538}$	13.65	33.28/41
13	X − 05 − 04	53312.736	$0.020^{+0.008}_{-0.002}$	$0.127^{+0.010}_{-0.024}$	$166.567^{+2.131}_{-2.107}$	$3.239^{+0.034}_{-0.033}$	$13.282^{+0.408}_{-0.395}$	13.65	31.35/41
14	X − 06 − 00	53314.749	$0.021^{+0.008}_{-0.002}$	$0.126^{+0.008}_{-0.022}$	$171.430^{+2.157}_{-1.788}$	$3.135^{+0.025}_{-0.032}$	$13.935^{+0.374}_{-0.364}$	13.65	18.94/41

accretion flow was primarily governed by a single component, i.e. the Keplerian flow. As a result, its spectrum is principally fitted by *diskbb* and the additional advective component is not needed. Since in TCAF we are interested to study the interplay between the two components, we concentrate on the declining phase during MJD = 53287.484–MJD = 53314.749 period.

4.1 Spectral data fitted by TCAF model

Table 1 illustrates the variation of the physical parameters, namely, the disc accretion rate ($\dot{m}_d$), the halo rate ($\dot{m}_h$), the shock location (X_s) that gives an indication of the size of the Compton cloud and the strength of the shock (R) with days (MJD) in the 2.5–25 keV (3–53 channels) energy band during the declining phase of the outburst. To explicitly show that the rates are independent, we also plot the ratio ARR(=$\dot{m}_h/\dot{m}_d$). The model normalization (N) is kept in the range 10–20. The average value of N ($N_{\rm avg}$) is determined and the same procedure is repeated for the constant value of $N = N_{\rm avg} = 13.65$, which we think is a good estimate of the normalization. If we ignore possible precession in the system, contribution from jets that have not been introduced in TCAF, and the possible change in shape with states, this can be treated as true normalization for the system. The spectral evolution of the rest of the parameters are shown in Table 2. The trends of variation of the flow parameters were found to be similar in both cases. Hence, we only discuss the spectral evolution for N in the range 10–20.

Spectral evolution of the declining phase and corresponding TCAF parameters:

(i) *HIMS*: for a period of ∼13 d, MJD = 53287.484 to MJD = 53300.208, the object seems to have remained in the HIMS that is evident from Table 1 and Fig. 4. During this period, the PCA flux consistently decreases as long as $\dot{m}_d$ is greater than $\dot{m}_h$, from

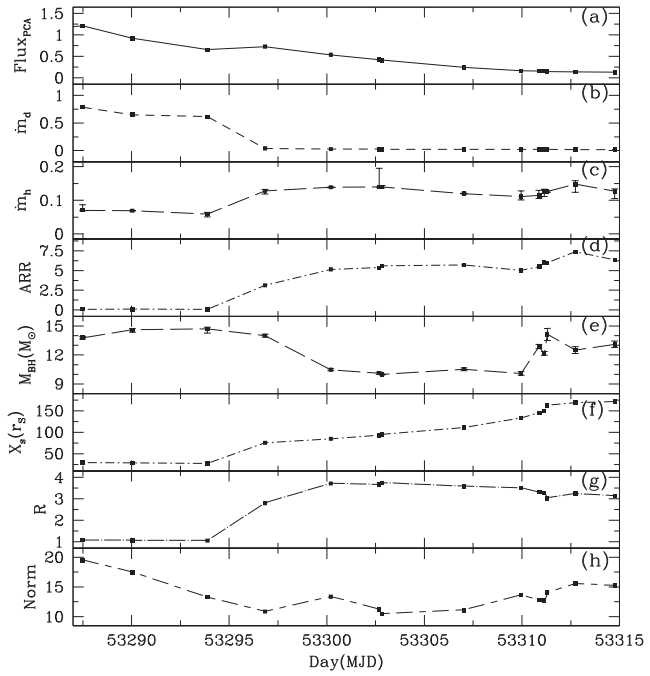

Figure 4. Variation of (a) the total PCA flux (in units of 10^{-9} ergs cm^{-2} s^{-1}), (b) the disc accretion rate $\dot{m}_d$ (in Eddington units), (c) the sub-Keplerian halo accretion rate $\dot{m}_h$ (in Eddington units), (d) the accretion rate ratio, ARR($=\dot{m}_h/\dot{m}_d$), (e) the mass of the BH (in units of $M_\odot$), (f) the shock location X_s (in units of r_S), (g) the shock strength R and (h) the normalization of the TCAF model, with day (MJD). Note that the normalization is restricted between 10and20 in the above fits. Variation of all the aforementioned quantities are studied in the 2.5–25 keV energy band. We have added error bars corresponding to Figs 4(c) and (e). The remaining error bars are too inconspicuous to be marked.

MJD = 53287.484 to MJD = 53293.882 and then remains roughly constant (Fig. 4a). On MJD = 53296.834, $\dot{m}_h$ becomes greater than $\dot{m}_d$ and shock suddenly moves outward from $X_s = 27.803 r_S$ to $X_s = 75.662 r_S$. During the HIMS to HS transition, on MJD = 53296.834 and MJD = 53300.208, QPOs were observed in the power density spectra (PDS). A typical spectra of this state, along with the unfolded models and residue is shown in Fig. 5(a).

(ii) *HS*: from the data in Table 1, it seems after MJD = 53300.208 the source entered in the HS and remained there till the end of the observation. A typical spectra of this state, along with the unfolded models and residue is shown in Fig. 5(b). The PCA flux also went down from this day and remained low till the end of the observation that is characteristic of the HS. This is evident from Fig. 4(a). No QPOs were observed in the power-density spectrum of the source during these days. The disc accretion rate that had fallen towards the end of the HIMS remains low (∼0.022) while the halo rate remains comparatively higher (∼0.13). The shock front moves further and further outward with time, from ∼75 r_S to ∼171 r_S, in a period of ∼14 d. The propagation of the shock front not only gives the clear picture as promised by the TCAF spectral fits, but also helps us to use another method of verifying the mass of the object by an independent method, namely, by the use of POS model (Chakrabarti et al. 2005, 2008; Debnath et al. 2010, 2013; Nandi et al. 2012). The spectral analysis restrict both mass and normalization in a narrow domain. We investigate below to check whether the same mass range is obtained from the timing analysis or not.

The mass was determined to be $\langle M_{\rm BH}\rangle = 12.36 \pm 1.73$ $M_\odot$, with an average $\langle \chi^2_{\rm red}\rangle = 0.82 \pm 0.20$ and the average normalization is found to be $N_{\rm avg} = 13.65 \pm 2.49$. The same process, when repeated by using a fixed $N = N_{\rm avg} = 13.65$, yielded similar results. These are shown in Fig. 6. The mass was determined to be $\langle M_{\rm BH}\rangle = 12.19 \pm 1.88$ $M_\odot$, with an average $\langle \chi^2_{\rm red}\rangle = 0.79 \pm 0.19$. The peak of the Gaussian line profile was close to the same value as that of the previous case.

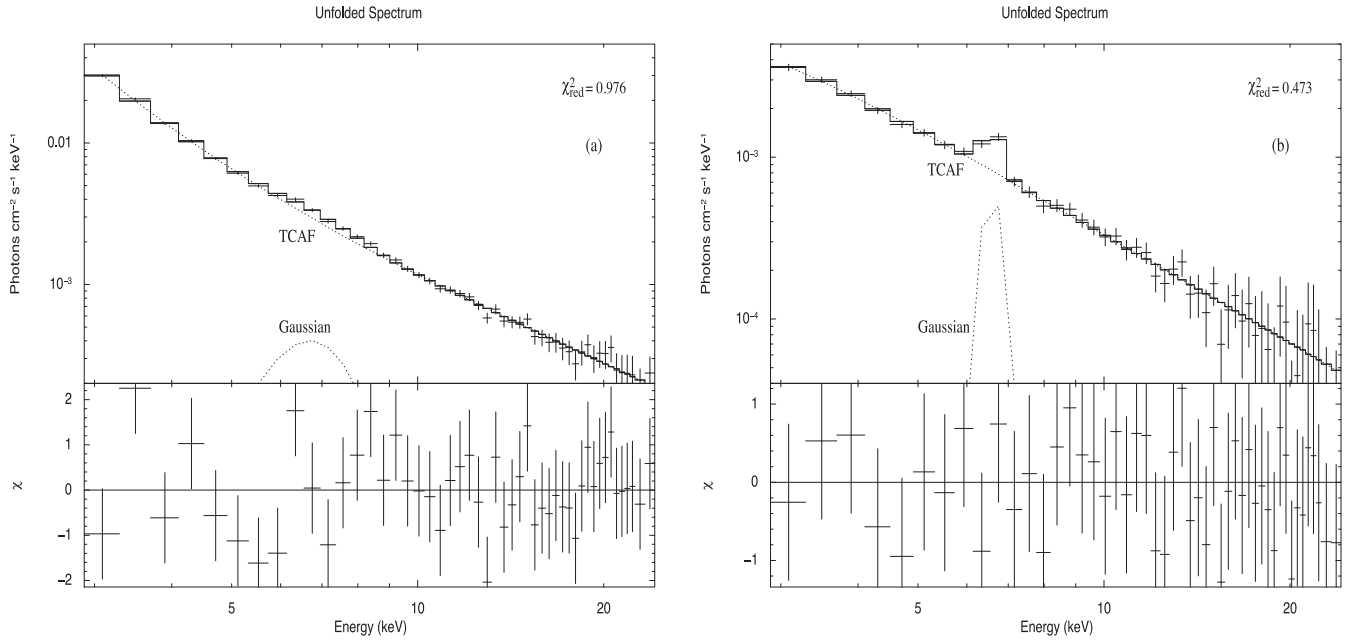

Figure 5. Unfolded spectra with residue of two observations [ID: 90115-01-03-00 (a) and 90115-01-06-00 (b)] for energy 2.5–25.0 keV, fitted with *wabs*(*TCAF*+*Gaussian*) models.

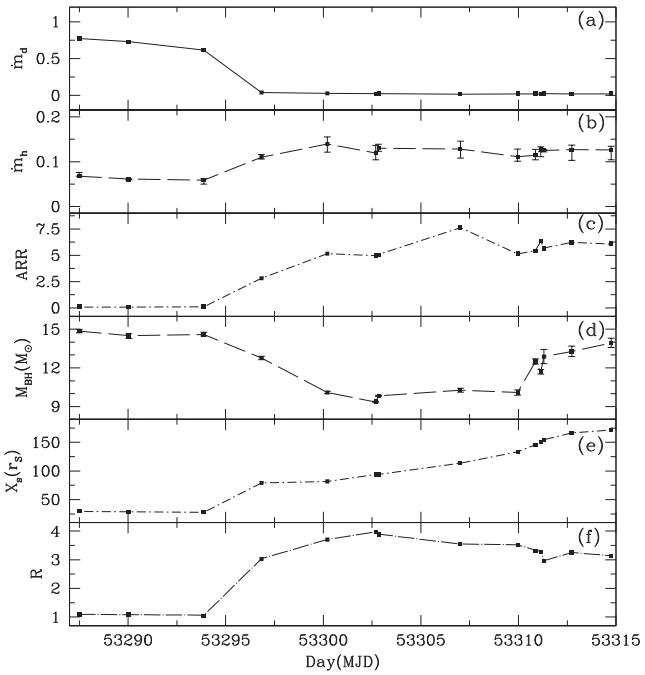

Figure 6. Variation of (a) the disc accretion rate $\dot{m}_d$ (in Eddington units), (b) the sub-Keplerian halo accretion rate $\dot{m}_h$ (in Eddington units), (c) the accretion rate ratio, ARR($=\dot{m}_h/\dot{m}_d$), (d) the mass of the BH (in units of $M_\odot$), (e) the shock location X_s (in units of r_S), (f) the shock strength R, with day (MJD). Variation of all the aforementioned quantities are studied in the 2.5–25 keV energy band keeping the normalization of the TCAF model fixed to $N = N_{\rm avg} = 13.65$. We have added error bars corresponding to Figs 6(b) and (d). The remaining error bars are too inconspicuous to be marked.

4.2 Correlating spectral and timing properties

Timing analysis was limited by the lack of observable low-frequency QPOs in the declining phase of the outburst. Out of the 14 data IDs, only 2 d showed prominent QPOs. We use this to determine the mass of the object separately. We use the POS model in determining the QPO frequencies from the spectral fit parameters, and use the same equations to obtain the value of mass, for which the deviation between the theoretical and observational QPO frequencies are minimum. We also determine inward velocity of the shock front for the first day of QPO observation to compare our results with previous works (Chakrabarti & Manickam 2000; Chakrabarti et al. 2009; Debnath et al. 2013).

Each PDS was analysed with a Lorentzian fit using the ftools commands. The values of the centroid frequency, full-width at half-maxima and peak power are obtained with 90 per cent confidence. From the values of $X_s, R, M_{\rm BH}$, the oscillation frequency of the shock front that is directly related to the frequency of the QPOs can be derived and compared to the frequency obtained independently from the analysis of the power density spectrum, $\nu_{\rm QPO}^{\rm PDS}$.

The QPO frequencies obtained from the POS model using the corresponding values of the TCAF parameters taken from Table 1, along with their respective systematic errors are given in Table 3, and is denoted by $\nu_{\rm qpo}^{\rm POS}$. The same calculation is repeated for the case with constant normalization, using the respective parameters from Table 2 and is reported in Table 4. We found that these two values agree with each other within the error bars.

Next, on MJD = 53296.834 and MJD = 53300.208, when QPOs were observed, we used the corresponding fit parameters X_s and R and varied the mass from 9 to 15 $M_\odot$ to calculate the corresponding QPO frequencies, $\nu_{\rm QPO}$. The chi-square of the distribution is calculated using $\nu_{\rm QPO}^{\rm PDS}$. The value of the mass for which the chi-square is minimum corresponds to $M_{\rm BH}^{\rm POS}$ that is quite close to the value of the mass obtained from the TCAF fits, $M_{\rm BH}$, on each of the days.

We calculated the velocity of the shock front for the first day (MJD = 53296) of QPO observation. The velocity of the shock front is $v_0 = 107.0^{+18.083}_{-18.083}$ cm s^{-1}, which is of the order of values found by Debnath et al. (2013). For the constant normalization case, it came out to be $v_0 = 31.6^{+16.146}_{-16.146}$ cm s^{-1}. This is in the same ball park for all the outburst sources GRO J1655-40 (Chakrabarti et al. 2005, 2008), XTE J1550-564 (Chakrabarti et al. 2009), GX 339-4 (Debnath et al. 2010; Nandi et al. 2012), H 1743-322 (Debnath et al. 2013) and IGR J17091-3624 (Iyer, Nandi & Mandal 2015) and is generally thought to be due to the change of pressure in CENBOL due to Compton cooling that drives the shock radially (Mondal, Chakrabarti & Debnath 2015). The deviation between these two approaches may be due to the fact that POS had only two points to fit the evolution of QPOs. With constant normalization, the position of the shock front does not change much during the two consecutive days that gives rise to a large systematic error in its measurement that is responsible for the discrepancy between the shock velocities in the two cases.

4.3 Mass estimation using the TCAF and POS model fits

The three different methods used in determining the mass of the BH, yield masses in the same range, up to the corresponding error bars. We obtain the average value of mass to be $\langle M_{\rm BH}\rangle = 12.36 \pm 1.73$ $M_\odot$, for spectral fits with free normalization. The average value of mass is found to be 12.19 ± 1.88 $M_\odot$, when the normalization is kept constant at $N = N_{\rm avg} = 13.65$. The POS model was applied to both the scenarios for both the observation IDs. In the first case, the masses obtained were 14.011 $M_\odot$ and 10.479 $M_\odot$, respectively. For the second case, the masses were 12.156 $M_\odot$ and 11.125 $M_\odot$, respectively. All four of these values lie within the range estimated by the spectral fits with constant normalization (10.31 $M_\odot$–14.07 $M_\odot$). Incidentally, M17 also obtained the average value of normalization $N \sim 15.55$ that lies within the range predicted by us. Our result conforms with the previous predictions of Shaposhnikov & Titarchuk (2009) and McClintock et al. (2009). However, both these methods use mass of other BHC as a reference to calculate mass of an unknown BH, but our method gives an independent method, where mass can be estimated even from one spectral fit using the TCAF solution. We do not require to know the mass of other BHCs to estimate mass of an unknown BHC. In Shaposhnikov & Titarchuk (2009), mass only can be predicted if there are sufficient observations in the transition and saturation branches of their QPO frequency–photon index correlation plot. Similarly, in high-frequency correlation method (used in McClintock et al. 2009), mass of those unknown BHCs can be predicted, which have shown signature of HFQPOs (so far only seven BHCs). These sources have shown multiple set (2:3) of HFQPOs.

The iron line emission profile was found to be peaked at around 6.5 keV for all the fits, with an average of 6.57 ± 0.13 keV. Fig. 4 shows variations of all the TCAF parameters with MJD. Thus, we find that the normalization N of the TCAF model does not change over a period of seven years i.e. from 2004 to 2011 indicating that probably the accretion disc is not precessing with significant amplitude.

Table 3. The spectral parameters from TCAF fits $M_{\rm BH}$, X_s and R are used in the formula obtained from POS for the determination of QPO frequency. The value is listed as $\nu_{\rm qpo}^{\rm POS}$ within error bars. The mass $M_{\rm BH}$ is then tuned further to reduce the difference between POS prediction and observed QPO $\nu_{\rm qpo}^{\rm PDS}$. The corresponding values is noted as $M_{\rm BH}^{\rm POS}$.

Comparison of QPO frequencies obtained from theoretical predictions and actual fits when N is in the range 10–20.							
Obs ID.	MJD	$M_{\rm BH}$ ($M_\odot$)	X_s (r_S)	R	$\nu_{\rm qpo}^{\rm POS}$(Hz)	$\nu_{\rm qpo}^{\rm PDS}$(Hz)	$M_{\rm BH}^{\rm POS}$ ($M_\odot$)
90115-01-03-10	53296.834	$13.995^{+0.151}_{-0.149}$	$75.662^{+0.704}_{-0.699}$	$2.804^{+0.010}_{-0.010}$	$3.957^{+0.112}_{-0.112}$	$3.952^{+0.157}_{-0.166}$	$14.011^{+0.602}_{-0.547}$
90115-01-04-00	53300.208	$10.476^{+0.091}_{-0.090}$	$84.784^{+1.265}_{-1.249}$	$3.717^{+0.046}_{-0.046}$	$3.359^{+0.145}_{-0.145}$	$3.358^{+0.208}_{-0.144}$	$10.479^{+0.460}_{-0.620}$

Table 4. Spectral parameters from TCAF fits $M_{\rm BH}$, X_s and R are used in POS model for the determination of QPO frequency. The value is listed as $\nu_{\rm qpo}^{\rm POS}$ within errors bars. The mass $M_{\rm BH}$ is then tuned further to reduce differences between POS prediction and observed QPO $\nu_{\rm qpo}^{\rm PDS}$. The corresponding value is noted as $M_{\rm BH}^{\rm POS}$.

Comparison of QPO frequencies obtained from theoretical predictions and actual fits keeping $N = N_{\rm avg} = 13.65$.							
Obs ID.	MJD	$M_{\rm BH}$ ($M_\odot$)	X_s (r_S)	R	$\nu_{\rm qpo}^{\rm POS}$(Hz)	$\nu_{\rm qpo}^{\rm PDS}$(Hz)	$M_{\rm BH}^{\rm POS}$ ($M_\odot$)
90115-01-03-10	53296.834	$12.772^{+0.127}_{-0.126}$	$79.041^{+0.494}_{-0.491}$	$3.026^{+0.016}_{-0.016}$	$3.758^{+0.092}_{-0.092}$	$3.952^{+0.157}_{-0.166}$	$12.156^{+0.521}_{-0.475}$
90115-01-04-00	53300.208	$10.095^{+0.082}_{-0.081}$	$81.732^{+1.278}_{-1.260}$	$3.700^{+0.046}_{-0.046}$	$3.697^{+0.162}_{-0.162}$	$3.358^{+0.208}_{-0.144}$	$11.125^{+0.487}_{-0.656}$

5 DISCUSSIONS AND CONCLUSIONS

In this paper, we investigate evolution of spectral properties of the Galactic BHC H1743-322 during the declining phase of the 2004 outburst to study the accretion flow dynamics and to extract the mass of the BH independently from each observation. This was the first 'normal' outburst after about 20 yr. However, data during hard and HIMSs in the rising phase are missing and since then it was mostly in SSs except towards the end of the declining phase. Hence, we concentrate our study only in this end phase as we expect interplay between the two flow components of TCAF models. We successfully addressed the evolution of accretion rates of both disc and halo, shock location (which represents the size of the Compton cloud) and the compression ratio to have a clear understanding of the outburst. It is important to note here that the fits obtained by spectral models, such as *diskbb + power law*, does not provide any clue about the mass of the object, neither does it explain the accretion flow dynamics around the BHC. TCAF solution, on the other hand, gives an independent estimate of $M_{\rm BH}$ from every single observation.

M17 obtained the mass of the BH in the range $11.2^{+1.66}_{-1.95}\,M_\odot$. Further, they estimated the mass of the BH with other methods such as Shaposhnikov & Titarchuk (2007, herefater ST07) using the photon index–QPO frequency correlation technique. The measured mass of the BH was obtained as $11.61 \pm 0.62\,M_\odot$. Shaposhnikov & Titarchuk (2009) predicted the mass of the BH to be $13.3 \pm 3.2\,M_\odot$ using the correlation between their spectral and timing properties while McClintock et al. (2009), estimated the mass $\sim$11.0 $M_\odot$ using their high-frequency QPO correlation method. From the model of high-frequency QPOs based on the spin of the BH Pétri (2008) obtained the mass of the BHC in the range of 9–13 $M_\odot$. We have obtained the mass of the BH in the range 10.31 $M_\odot$–14.07 $M_\odot$ that agrees well with these previous measurements.

The PCA spectra of the object clearly show that most of the flux is contributed from the soft photons emitted by the disc. The flux emitted from the disc is $\sim T^4$ and draws its energy from the loss in gravitational potential energy $\sim \frac{GM_{\rm BH}}{r}$. Thus, roughly the spectra obtained by the best fit with TCAF has an intrinsic dependence of T on $M_{\rm BH}$ as $M_{\rm BH} \sim T^4$. The spectra at low energy, where the blackbody radiation from the disc is dominating, is limited by the resolution of *RXTE*/PCA. Any error in the measurement, combined with the error in the fit parameters that depend on T, leads to a significant proportional error in the determination of $M_{\rm BH}$. Despite that, the mass is found to lie in a narrow range that conforms and restricts further, the previous findings by M17 and Pétri (2008).

We assumed that the mass, distance and inclination angle of the object are constant such that the projected area of the disc along the line of sight does not change keeping the model normalization more or less unchanged provided the instrument response function and the absorption from intervening medium are determined correctly that may affect normalization also. Furthermore, we assumed that there was no contribution to X-rays from the jet. However, since mass, distance or inclination angle are not accurately known and the *RXTE* resolution is low to generate accurate spectra, we allowed to vary both mass and normalization within a narrow range. We also used the average normalization and repeated our analysis. We found reasonably good reduced χ^2 values as evident from Tables 1 and 2. The average reduced *chi*^{2} value is $\langle\chi^2_{\rm red}\rangle = 0.82 \pm 0.20$ for $10 < N < 20$ and $\langle\chi^2_{\rm red}\rangle = 0.79 \pm 0.19$ for $N = N_{\rm avg} = 13.65$. We believe that unless the system parameters (most importantly inclination angle for a precessing disc) change, this Normalization may be used to analyse subsequent outbursts.

The low frequency of QPO derived from the power density spectrum fitted parameters was found to be in agreement with the one obtained from the POS model if the systematic error is considered. The velocity of the shock front v_s using the POS model was found to be similar to those with the previous work by Debnath et al. (2013).

The masses obtained by the POS model for both the cases with free and constant normalization agree with the range (10.31 $M_\odot$–14.07 $M_\odot$) obtained by the spectral fits with a constant, averaged normalization of $N = N_{\rm avg} = 13.65$. The POS model provides a secondary verification to our method and reflects upon the general consistency of our approach. We thus conclude from our analysis that the mass of the BHC is in the range 10.31 $M_\odot$–14.07 $M_\odot$.

TCAF solves the radiative transfer equation for a steady state two component flow to discuss about the spectral properties. The day-to-day evolution of the spectra are, thus, explained in terms of the variation of physical parameters that are used in TCAF. This

allows us to have a fresh estimate of the mass of the BH, independent of any other observations. The POS model predicts values of QPO frequencies from the spectral parameters, and we find that observed QPOs are of similar values. Thus TCAF self-consistently puts spectral and timing properties under a common framework. The derived mass is well within the range estimated by earlier workers using very different observational data, and model. Presently, TCAF does not incorporate effects of magnetic fields, spin of the BH or line emissions. These effects are being incorporated and results would be reported elsewhere.

ACKNOWLEDGEMENTS

DD acknowledges support from the ISRO sponsored RESPOND project fund (ISRO/RES/2/388/2014-15). IB acknowledges the support from SNBNCBS-PDRA Fellowship.

REFERENCES

Arnaud K. A., 1996, in Jacoby G. H., Barnes J., eds, ASP Conf. Ser. Vol. 101, Astronomical Data Analysis Software and Systems V. Astron. Soc. Pac., San Francisco, p. 17
Belloni T., Homan J., Casella P., van der Klis M., Nespoli E., Lewin W. H. G., Miller J. M., Mendez M., 2005, A&A, 440, 207
Cambier H. J., Smith D. M., 2013, ApJ, 767, 46
Capitanio F. et al., 2005, ApJ, 622, 503
Capitanio F., Belloni T., Del Santo M., Ubertini P., 2009, MNRAS, 398, 1194
Chakrabarti S. K., 1989, MNRAS, 240, 7 (C89)
Chakrabarti S. K., 1990, Theory of Transonic Astrophysical Flows. World Scientific Press, Singapore (C90)
Chakrabarti S. K., 1996, ApJ, 464, 66d4 (C96)
Chakrabarti S. K., 1997, ApJ, 484, 313
Chakrabarti S. K., 2016, in Ruffini R., Jantzen R., Bianchi M., eds, Proc. 14th Marcel Grossman meeting. Study of Accretion processes Around Black Holes becomes Science: Tell Tale Observational Signatures of Two Component Advective Flows. World Scientific Press, Singapore
Chakrabarti S. K., Manickam S. G., 2000, ApJ, 531, L41
Chakrabarti S. K., Titarchuk L. G., 1995, ApJ, 455, 623 (CT95)
Chakrabarti S. K., Nandi A., Debnath D., Sarkar R., Datta B. G., 2005, Indian J. Phys., 79, 841 (astro-ph/0508024)
Chakrabarti S. K., Debnath D., Nandi A., Pal P. S., 2008, A&A, 489, L41
Chakrabarti S. K., Dutta B. G., Pal P. S., 2009, MNRAS, 394, 1463
Chakrabarti S. K., Mondal S., Debnath D., 2015, MNRAS, 452, 3451
Chatterjee D., Debnath D., Chakrabarti S. K., Mondal S., Jana A., 2016, ApJ, 827, 88
Cooke B. A., Levine A. M., Lang F. L., Primini F. A., Lewin W. H. G., 1984, ApJ, 285, 258
Coriat et al., 2011, MNRAS, 414, 677
Debnath D., Chakrabarti S. K., Nandi A., Mandal S., 2008, Bull. Astron. Soc. India, 36, 151
Debnath D., Chakrabarti S. K., Nandi A., 2010, A&A, 520, 98
Debnath D., Chakrabarti S. K., Nandi A., 2013, Adv. Space Res., 52, 2143
Debnath D., Mondal S., Chakrabarti S. K., 2014, MNRAS, 440, L121
Debnath D., Mondal S., Chakrabarti S. K., 2015a, MNRAS, 447, 1984
Debnath D., Molla A. A., Chakrabarti S. K., Mondal S., 2015b, ApJ, 803, 59
Doxsey R. et al., 1977, IAU Circ., 3113, 2
Emelyanov A. N., Aleksandrovich N. L., Sunyaev R. A., 2000, Astron. Lett., 26, 297
Galeev A. A., Rosner R., Vaiana G. S., 1979, ApJ, 229, 318
Ghosh H., Garain S. K., Giri K., Chakrabarti S. K., 2011, MNRAS, 416, 959
Giri K., Chakrabarti S. K., 2013, MNRAS, 430, 2836
Gursky H. et al., 1978, ApJ, 223, 973
Haardt F., Maraschi L., 1993, ApJ, 413, 507
Iyer N., Nandi A., Mandal S., 2015, ApJ, 807, 108
Jana A., Debnath D., Chakrabarti S. K., Mondal S., Molla A. A., 2016, ApJ, 819, 107
Kaluzienski L. J., Holt S. S., 1977, IAU Circ., 3099, 3
McClintock J. E., Remillard R. A., 2006, in Lewin W., van der Klis M., eds, Compact Stellar X-ray Sources. Cambridge Univ. Press, Cambridge, p. 157
McClintock J. E. et al., 2009, ApJ, 698, 1398
Markwardt C. B., Swank J. H., 2003, Astron. Telegram, 133, 1
Miller-Jones J. C. A. et al., 2012, MNRAS, 421, 468
Molla A. A., Chakrabarti S. K., Debnath D., Mondal S., 2017, ApJ, 834, 88 (M17)
Molla A. A., Debnath D., Chakrabarti S. K., Mondal S., Jana A., 2016, MNRAS, 460, 3163 (M16)
Mondal S., Chakrabarti S. K., 2013, MNRAS, 431, 2716
Mondal S., Debnath D., Chakrabarti S. K., 2014, ApJ, 786, 4
Mondal S., Chakrabarti S. K., Debnath D., 2015, ApJ, 798, 57
Mondal S., Chakrabarti S. K., Debnath D., 2016, Ap&SS, 361, 309
Nandi A., Debnath D., Mandal S., Chakrabarti S. K., 2012, A&A, 542, 56
Parmar A. N., Kuulkers E., Oosterbroek T., Barr P., Much R., Orr A., Williams O. R., Winkler C., 2003, A&A, 411, L421
Pétri J., 2008, Ap&SS, 318, 181
Raynolds S. P., 1999, Astrophys. Lett. Commun., 38, 425
Remillard R. A., McClintock J. E., 2006, ARA&A, 44, 49
Revnivtsev M., Chernyakova M., Capitanio F., Westergaard N. J., Shoenfelder V., Gehrels N., Winkler C., 2003, Astron. Lett., 132, 1
Rupen M. P., Mioduszewski A. J., Dhawan V., 2003, Astron. Lett., 137, 1
Shakura N. I., Sunyaev R. A., 1973, A&A, 24, 337 (SS73)
Shaposhnikov N., 2010, Astron. Telegram, 2857, 1
Shaposhnikov N., Tomsick J. A., 2010, Astron. Lett., 2410, 1
Smith D., Heindl W. A., Swank J. H., 2002, ApJ, 569, 362
Soria R., Wu K., Hannikainen D., McMollough M., Hunstead R., 2001, in Yaqoob T., Krolik J. H., eds, X-Ray emission from Accretion on to Black Holes. p. 65, preprint (astro-ph/0108084)
Steeghs D., Miller J. M., Kaplan D., Rupen M., 2003, Astron. Telegram, 146, 1
Steiner J. F., McClintock J. E., Reid M. J., 2012, ApJ, 745, L7
Sunyaev R. A., Titarchuk L. G., 1980, ApJ, 86, 121
Sunyaev R. A., Titarchuk L. G., 1985, A&A, 143, 374
Tomsick J. A., Yamaoka K., Corbel S., Kalemci E., Migliari S., Kaaret P., 2014, ApJ, 791, 70
White N. E., Marshall F. E., 1984, ApJ, 281, 354
Wu K. et al., 2002, ApJ, 565, 1161
Zdziarski A. A., Lubiński P., Gilfanov M., Revnivtsev M., 2003, MNRAS, 342, 355

This paper has been typeset from a TEX/LATEX file prepared by the author.